Chapter 5

Optimization Design of Nonlinear Optical Frequency Conversion Devices Using Simulated Annealing Algorithm

Yan Zhang

Additional information is available at the end of the chapter

http://dx.doi.org/10.5772/50074

1. Introduction

Laser has become to be a fundamental light source in modern communication, scientific research, and industrial applications. More and more laser frequencies are required for various applications. However, common laser crystals can provide only some fixed frequencies which cannot satisfy various requirement. Nonlinear optical process presents an alternative approach for generating rich laser frequencies. The traditional nonlinear optical processes usually require the so called phase-matching condition [1, 2], which requires the nonlinear optical crystals with birefringence. The phase-matching condition raises a restriction of the choice of natural birefringence materials in the applications of frequency conversion. Quasi-phase-matching method uses periodic modulation of the nonlinear property of a crystal to compensate the mismatch between the wave vectors of the interaction light beams [3]. This method allows utilization of the large component of the nonlinear susceptibility tensor, which is usually inaccessible with the common phase matching. Periodic optical superlattice provides a reciprocal vector to compensate the phase mismatch between the interacting light beams. Thus, only one nonlinear process can be performed in the periodic optical superlattice. This idea can be naturedly expended to the aperiodic optical supperlattice which can provide a series of reciprocal vectors. The reciprocal vectors can be preset for special nonlinear process. The key problem is how to design different aperiodic optical supperlattice for matching the specified nonlinear optical process with high conversion efficiency.

In this chapter, the simulated annealing (SA) method is used to successfully design nonlinear optical frequency conversion devices for achieving different nonlinear optical processes, for example, multiple second harmonics generation and coupled third harmonic generation in the aperiodic optical superlattice, multiple wavelengths parametric amplification, multiple wavelengths second harmonics generation and coupled third harmonic generation in the defective nonlinear photonic crystals. The simulation results demonstrate that the SA method is an effective algorithm for nonlinear optical frequency conversion devices design. The designed devices can archive the preset goal well.

2. Design of aperiodic optical supperlattice

Unlike the periodic optical supperlattice, the aperiodic optical superlattice can provide more spatial Fourier components of structure, therefore, some coupled parametric processes may be realized in this kind of devices. Firstly, the optimal design problem of the aperiodic optical superlattice is described in the real-space representation. Then several model designs are carried out to demonstrate the effectiveness of the present design method. The $LiTaO_3$ is selected as basic crystal for polarizing. The direction of polarization vectors in successive domain are opposite, thus are the signs of the nonlinear optical coefficients. However, the width of each individual domain is no longer equal and should be determined by the specified nonlinear optical processes.

2.1. Design method

We use the second harmonic generation (SHG) process for a single wavelength as an example. Assume that a laser beam with frequency $\omega_1 = \omega$ is perpendicularly incident on the surface of an aperiodic optical superlattice. In order to use the largest nonlinear coefficient d_{33}, let the propagation and polarization directions of the input light are along the x and z axes, respectively. Two optical fields are involved in the SHG process. one is the fundamental wave with $\omega_1 = \omega$ and other is the second harmonic wave with $\omega_2 = 2\omega$. Under the slowing-wave and small-signal approximations, the conversion efficiency η_{SHG} from the fundamental wave to second harmonic wave can be written as:

$$\eta_{SHG} = \frac{I_{2\omega}}{I_\omega} = \frac{8\pi^2 |d_{33}|^2 I_\omega L^2}{c\epsilon_0 \lambda^2 n_{2\omega} n_\omega^2} \left| \frac{1}{L} \int_0^L e^{i(k_{2\omega} - 2k_\omega)x} \tilde{d}(x) dx \right|^2, \tag{1}$$

where $k_\omega = n_\omega \omega / c$ ($k_{2\omega} = n_{2\omega} 2\omega / c$) is the wave number of the fundamental (second harmonic) wave, c is the speed of light in vacuum, n_ω ($n_{2\omega}$) is the refractive index of crystal at the fundamental (second harmonic) wavelength, ε_0 is the permittivity of vacuum, and L is the total length of the sample. I_ω ($I_{2\omega}$) is the intensity of the fundamental (second harmonic) wave beam, and $\tilde{d}(x)$ only takes binary values of 1 or -1 which depends on the polarization direction. The coherence length $l_c^{(s)}(\lambda)$ for the SHG is defined as:

$$l_c^{(s)}(\lambda) = \frac{2\pi}{\Delta k} = \frac{2\pi}{k_{2\omega} - 2k_\omega} = \frac{\lambda}{2(n_{2\omega} - n_\omega)}. \tag{2}$$

Thus Equation 1 can be rewritten as

$$\eta_{SHG} = C_s C^2(\lambda) \xi_{eff}^{(s)2}(s), \tag{3}$$

with

$$C_s = \frac{8\pi^2 |d_{33}|^2 I_\omega L^2}{c\varepsilon_0}, \tag{4}$$

$$C(\lambda) = \frac{1}{\lambda \sqrt{n_{2\omega}} n_\omega}, \tag{5}$$

and

$$\xi_{eff}^{(s)}(\lambda) = \left| \frac{1}{L} \int_0^L e^{i(2\pi x / l_c^{(s)}(\lambda))} \tilde{d}(x) dx \right|, \tag{6}$$

the parameter $\xi_{eff}^{(s)}(\lambda)$ depends on the polarization direction of each domain.

Assume that the thickness of the each domain of the aperiodic optical superlattice is Δx, thus the number of blocks in the sample is $N = L/\Delta x$. The position of each domain is $x_q = q\Delta x$ for $q = 0, 1, 2, ...(N-1)$. Equation 6 can be evaluated as

$$\begin{aligned} \xi_{eff}^{(s)}(\lambda) &= \frac{1}{N\Delta x}\left|\sum_{q=0}^{N-1}\tilde{d}(x_q)\int_{x_q}^{x_q+\Delta x} e^{i(2\pi x/l_c^{(s)}(\lambda))}dx\right| \\ &= \left|sinc\left[\frac{\Delta x}{l_c^{(s)}(\lambda)}\right]\right|\left|\left\{\frac{1}{N}\sum_{q=0}^{N-1}\tilde{d}(x_q)e^{i[2\pi(q+0.5)\Delta x/l_c^{(s)}(\lambda)]}\right\}\right|, \end{aligned} \tag{7}$$

where $sinc(x) = sin(\pi x)/(\pi x)$. It can be seen that $\xi_{eff}^{(s)}(\lambda)$ has two contributions: one belongs to the unit block and depends on the Δx and the coherence length $l_c^{(s)}(\lambda)$; the other is caused by the interference effect among the blocks and depends on the configuration of domains and the polarization direction of each block.

The optimization design of the aperiodic optical superlattice for the SHG can be ascribed as a search for the maximum of $\xi_{eff}^{(s)}(\lambda)$ with respect to $\tilde{d}(q\Delta x)$. The first factor in Equation 7 has its maximum value $2/[\pi(2m+1)]$ when $\Delta x = [(2m+1)/2]l_c^{(s)}(\lambda)$. The second factor has its maximum value of 1 in the case of the periodic structure with a period of $a = 2\Delta x = l_c^{(s)}(\lambda)$, $d(x_q)$ takes opposite sign between two consecutive blocks. In this case, the phase lagging factor perfectly matches the reversal of the domain orientation between two adjacent blocks and the ideal constructive interference emerges. However, in the case of the aperiodic structure, it is quite difficult to find a solution and can be solved with the SA algorithm.

In order to demonstrate the effectiveness of the SA algorithm for design of aperiodic optical superlattices, a simple example of a single wavelength SHG is considered here. The parameters are chosen as follows: the wavelegth of the incident beam is $\lambda = 1.064\mu m$, the thickness of the unit block is $\Delta x = l_c^{(s)}(\lambda)/2 = 3.8713\mu m$, and the number of blocks is 2142. Thus the total length of sample is $L = 8298.8\mu m$. The refractive indexes of material at corresponding wavelengths are evaluated by the Sellmeier equation [4]. The objective function in the SA algorithm is chosen as

$$E = |\xi^0 - \xi_{eff}^{(s)}(\lambda)|, \tag{8}$$

where ξ^0 is a preset value in guiding the SA procedure. Fig. 1 sketches a flowchart of the SA algorithm for constructing aperiodic optical superlattice. As shown in Fig. 1, the initial temperature and dropping rate are selected at the beginning of program, a random sign modulation $\tilde{d}(x_i)$ is substituted into Equation 8 to calculate the initial object function E_0. A new object function E_1 is calculated with changing the sign of a unit block in $\widetilde{d}(x_i)$ and the difference $\Delta E = E_1 - E_0$ is obtained. A random number $p, 0 \leq p \leq 1$, is generated by the computer. If p satisfies $p \leq \exp(-\Delta E/T)$, this change will be accepted and E_0 will be replaced by E_1, else the sign of this unit block will be retrieved and E_0 does not change. After test all of blocks, this procedure will be repeated with a new temperature $T = T \times \Delta T$ until no sign changes in the $\tilde{d}(x)$. Thus, the stable modulation left is the optimal one.

Finally, a perfect periodical structure with a pari of antiparallel domains for each unit block and with a period of $a = 2\Delta x = l_c^{(s)}$ as expected can be obtained. The reduced effective

nonlinear coefficient $\xi_{eff}^{(s)}$ reaches its theoretical maximum value of $2/\pi = 0.6366$. This means that the SA algorithm is appropriate for dealing with the above mentioned inverse source problem.

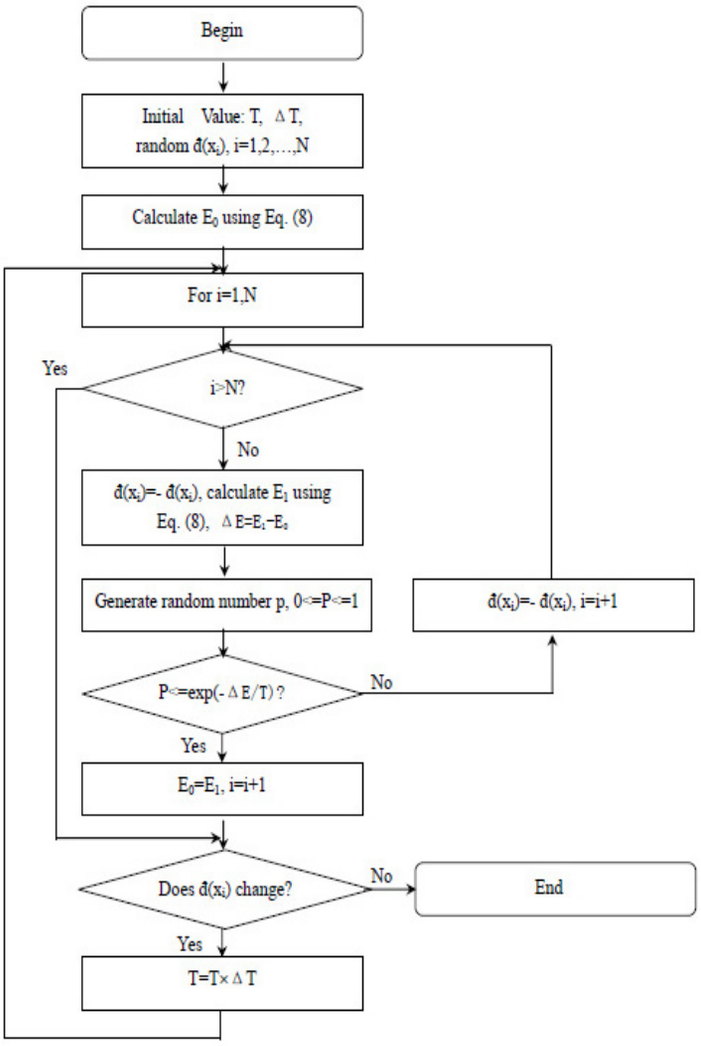

Figure 1. Flowchart of the SA algorithm for designing aperiodic optical superlattice.

2.2. Multiple wavelength SHG

A particular design of the aperiodic optical supperlattice is carried out. It is expected that it can implement multiple wavelength SHG with an identical effective nonlinear coefficient $\xi_{eff}^{(s)}(\lambda_\alpha) = \xi^0$ with ξ^0 is a constant. The thickness of each layer $\Delta x = 3.0\mu m$ for matching the state of the art of microfabrication in practice. The objective function in the SA algorithm is set as

$$E = \sum_{\alpha}[|\xi^0 - \xi_{eff}^{(s)}(\lambda_\alpha)|] + \beta[\max\{\xi_{eff}^{(s)}(\lambda_\alpha)\} - \min\{\xi_{eff}^{(s)}(\lambda_\alpha)\}], \tag{9}$$

where the function max{...} (min{...}) manifests to take their maximum (minimum) value among all the quantities including into {...}. β is an adjustable parameter taking a value

of $0.3-3$. Five wavelengths are $0.972\mu m$, $1.082\mu m$, $1.283\mu m$, $1.364\mu m$, and $1.568\mu m$. Other parameters are selected as: the total length of the sample $L = 8295\mu m$, the number of blocks $N = 2765$, and the wavelength sampling interval is $1nm$.

The obtained results are shown in Fig. 2. The wavelength is scanned with a interval of $0.05nm$ which is much small than that in the design procedure. There exist six strong peaks with almost identical peak value. Five of them are located at the expected wavelengths. One strong peak with an unexpected wavelength $\lambda = 0.981\mu m$ appears very close to the expected wavelength $\lambda = 0.972\mu m$. There are also some stray peaks appearing in the lower wavelength regions and small dense oscillation structures as a background. The average value of $\xi_{eff}^{(s)}(\lambda_\alpha)$ for preset five peaks is 0.1927 and the nonuniformity is 3.18×10^{-4}.

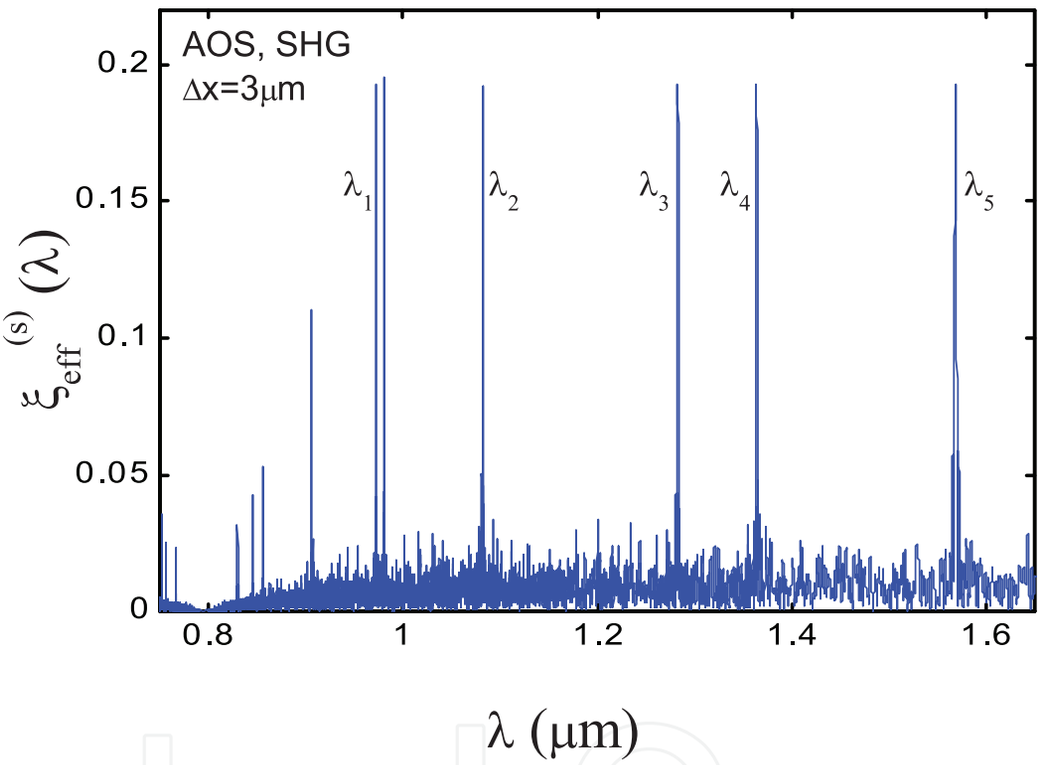

Figure 2. Calculated results for the constructed aperiodic optical superlattice that implements multiple wavelengths SHG with an identical nonlinear optical coefficient.

In order to further reveal the characteristic of the SHG in the constructed aperiodic optical superlattic, the plot of the variation of $\xi_{eff}^{(s)}(\lambda_\alpha)$ with the optical propagating distance x from the imping surface of incident light is shown in Fig. 3. It can be obviously seen that all curves exhibit nearly linearly increasing behavior with a nearly identical slope, which hints that the arrangement of domains is relatively favorable to the SHG process. The individual contribution is accumulated with each in the constructive interference state.

2.3. Coupled third harmonic generation for multiple wavelengths

Third harmonic generation (THG) has a wide application as a mean to extend coherent light sources to the short wavelengths. THG can be directly created using a third-order

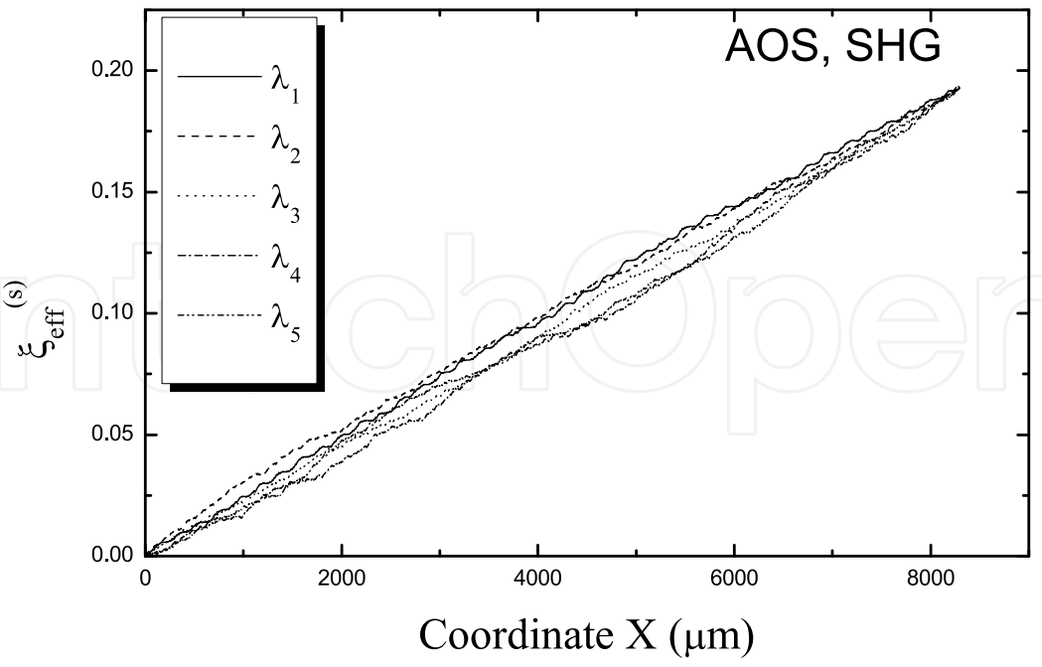

Figure 3. Variation of $\xi_{eff}^{(s)}(\lambda_\alpha)$ with the optical propagating distance x.

nonlinear process, however, this method is of little practical importance because of intrinsic weak third-order optical nonlinearity. An efficient THG can be achieved by cascading two second-order nonlinear process. Two nonlinear optical crystal are involved: the first one is for SGH and the second one for sum frequency generation. THG can also be generated form the coupled parametric processess with high efficiency. The coupled THG (CTHG) is raised from the coupling effect of two nonlinear optical precesses: one is the SHG and the other is a sum frequency process. This two processes couple with each other in a single crystal. This coupling leads to a continuous energy transfer from the fundamental to the second, and then to the third harmonic fields. Thus, a direct third harmonic wave can be generated with high efficiency.

The THG process can be analyzed by solving the coupled nonlinear equations that describe interaction of these three fields: E_ω, $E_{2\omega}$, and $E_{3\omega}$ in the aperiodic optical superlattice. Under the small signal approximation, the third harmonic wave conversion efficiency is expressed by

$$\eta_{THG} = \frac{I_{3\omega}}{I_\omega} = \frac{144\pi^4|d_{33}|^4 I_\omega^2 L^4}{c^2\epsilon_0^2\lambda^4 n_{3\omega}n_{2\omega}^2 n_\omega^3}\left|\frac{2}{L^2}\int_0^L e^{i(k_{3\omega}-k_{2\omega}-k_\omega)x}\tilde{d}(x)\int_0^x e^{i(k_{2\omega}-2k_\omega\zeta}\tilde{d}(\zeta)d\zeta dx\right|^2. \quad (10)$$

The coherence length $l_c^{(t)}(\lambda)$ for the CTHG is defined as

$$l_c^{(t)}(\lambda) = \frac{2\pi}{k_{3\omega}-k_{2\omega}-k_\omega} = \frac{\lambda}{(3n_{3\omega}-2n_{2\omega}-n_\omega)}. \quad (11)$$

Thus, Equation 10 can be rewritten as

$$\eta_{THG} = C_t C'^2(\lambda)(\xi_{eff}^{(ct)}(\lambda))^2, \quad (12)$$

with

$$C_t = \frac{144\pi^4 |d_{33}|^4 I_\omega^2 L^4}{c^2 \epsilon_0^2}, \tag{13}$$

$$C^{'}(\lambda) = \frac{1}{\lambda^2 n_\omega^{3/2} n_{2\omega} \sqrt{n_{3\omega}}}, \tag{14}$$

and

$$\xi_{eff}^{(ct)}(\lambda) = \left| \frac{2}{L^2} \int_0^L e^{i[2\pi x / l_c^{(t)}(\lambda)]} \tilde{d}(x) dx \int_0^x e^{i[2\pi \zeta / l_c^{(s)}(\lambda)]} \tilde{d}(\zeta) d\zeta \right|. \tag{15}$$

The variable $\xi_{eff}^{(ct)}(\lambda)$ is the reduced coupled effective nonlinear coefficient for the CTHG.

Assuming that the thickness of unit block is Δx, the number of the blocks in sample is $N = L/\Delta x$. The position of blocks is coordinated with $x_q = q\Delta x$, for $q = 0, 1, 2, 3...(N-1)$. Equation 15 will be rewritten as

$$\begin{aligned}
\xi_{eff}^{(ct)}(\lambda) &= \left| \frac{2}{(N\Delta x)^2} \sum_{q=0}^{N-1} \widetilde{d}(x_q) \int_{x_q}^{x_q+\Delta x} dx e^{i[2\pi x / l_c^{(t)}(\lambda)]} \sum_{p=0}^{q} \widetilde{d}(x_p) \int_{x_p}^{x_p+\Delta x} d\zeta e^{i[2\pi \zeta / l_c^{(s)}(\lambda)]} \right| \\
&= 2 \left| \left[\frac{1}{\Delta x} \int_0^{\Delta x} dx e^{i[2\pi x / l_c^{(t)}(\lambda)]} \right] \left[\frac{1}{\Delta x} \int_0^{\Delta x} d\zeta e^{i[2\pi \zeta / l_c^{(s)}(\lambda)]} \right] \right. \\
&\quad \left. \times \left\{ \frac{1}{N} \sum_{q=0}^{N-1} \widetilde{d}(x_q) e^{i[2\pi x_q / l_c^{(t)}(\lambda)]} \left[\frac{1}{N} \sum_{p=0}^{q-1} \widetilde{d}(x_p) e^{i[2\pi x_p / l_c^{(s)}(\lambda)]} \right] \right\} + \Delta u \right| \\
&= 2 \left| \left\{ sinc \left[\frac{\pi \Delta x}{l_c^{(t)}(\lambda)} \right] sinc \left[\frac{\pi \Delta x}{l_c^{(s)}(\lambda)} \right] \right\} \right. \\
&\quad \left. \times \left\{ \frac{1}{N^2} \sum_{q=0}^{N-1} \widetilde{d}(x_q) e^{i[2\pi (q+0.5)\Delta x / l_c^{(t)}(\lambda)]} \left[\sum_{p=0}^{q-1} \widetilde{d}(x_p) e^{i[2\pi (p+0.5)\Delta x / l_c^{(s)}(\lambda)]} \right] \right\} + \Delta u \right|,
\end{aligned} \tag{16}$$

with

$$\begin{aligned}
\Delta u &= \frac{2}{L^2} \sum_{q=0}^{N-1} \widetilde{d}(x_q) \int_{x_q}^{x_{q+1}} dx e^{i[2\pi x_q / l_c^{(t)}(\lambda)]} \int_{x_q}^{x} d\zeta e^{i[2\pi \zeta / l_c^{(s)}(\lambda)]} \\
&= \frac{1}{N^2} \left(\frac{l_c^{(s)}(\lambda)}{i\pi \Delta x} \right) \left\{ e^{\frac{i\pi \Delta x}{l_c^{(s)}(\lambda)} + \frac{i\pi \Delta x}{l_c^{(t)}(\lambda)}} sinc \left[\frac{\Delta x}{l_c^{(s)}(\lambda)} + \frac{\Delta x}{l_c^{(t)}(\lambda)} \right] - e^{\frac{i\pi \Delta x}{l_c^{(t)}(\lambda)}} sinc \left[\frac{\Delta x}{l_c^{(t)}(\lambda)} \right] \right\} \\
&\quad \times \sum_{q=0}^{N-1} e^{i[2\pi x_q (1/l_c^{(s)}(\lambda) + 1/l_c^{(t)}(\lambda)]}
\end{aligned} \tag{17}$$

From Equation 16, it can been found that $\xi_{eff}^{(ct)}(\lambda)$ has the contributions from two factors: one factor (double *sinc* functions) belongs to unit block and strongly depends on Δx and the coherence length $l_c^{(t,s)}(\lambda)$; the other factor which is included inside the second curly braces reflects the interference effect among the blocks in sample, depending on the arrangement of domains and the phase lagging from one block to other block. Δu contributes to a small correction.

A model design of the AOS that achieves the coupled THG is carried out. The parameters used in the design are : $\Delta x = 3\mu m$, $L = 8067\mu m$, $N = 2689$, and $\lambda = 1.570\mu m$. Fig. 4 displays the calculated results. The wavelength is scanned with an interval of $0.1nm$. There exists only one strong sharp peak at the preset wavelength of $\lambda = 1.570\mu m$ with $\xi_{eff}^{(ct)} = 0.1811$. It can be found that the designed structure performs the preset goal well.

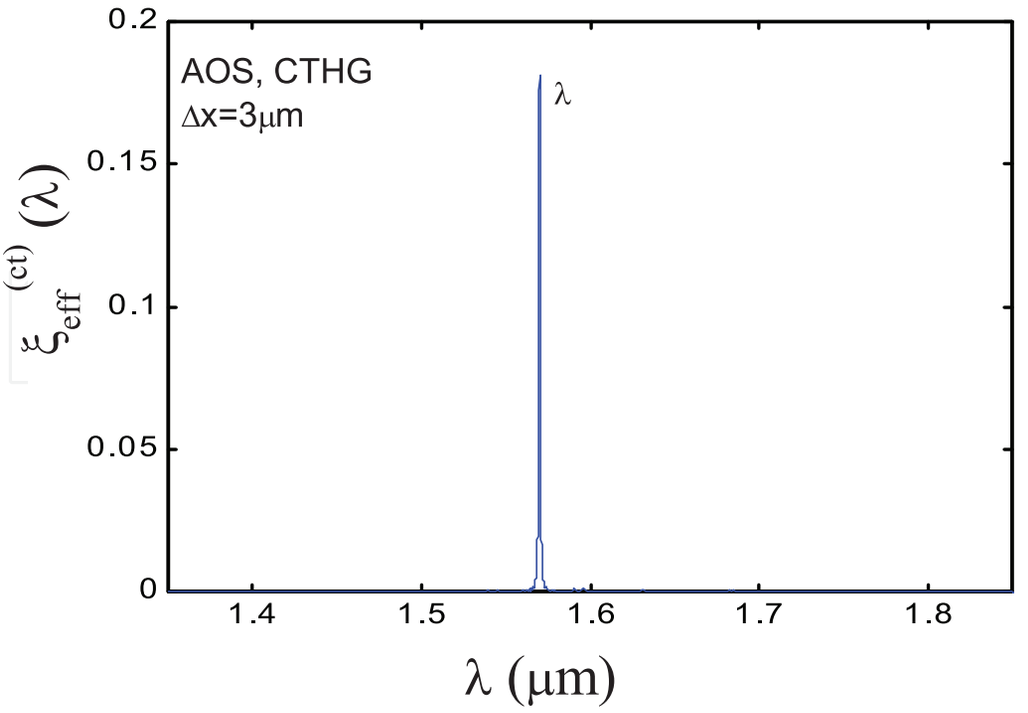

Figure 4. Calculated result for the constructed aperiodic optical superlattice that implements the CTHG.

The same method can be used to construct aperiodic optical superlattic that implements multiple wavelengths CTHG with identical effective nonlinear coefficient. The relevant parameters are: $\lambda_\alpha = [1.40, 1.60, 1.80]\ \mu m$, $\Delta x = 3\mu m$, $L = 8067\mu m$, and $N = 2689$. The dependence of $\xi_{eff}^{(ct)}(\lambda)$ on the wavelength is depicted in Fig. 5. The behavior of $\xi_{eff}^{(ct)}(\lambda)$ exhibits fairly good uniformity. The coupled effective nonlinear coefficient is almost identical for three different wavelengths and the average value is 0.04792.

2.4. Multiple wavelengths parametric amplification

Parametric generation provides unique possibility of generating widely tunable radiation from a single pump light source, so it has attracted extensive interest since parametric amplification was theoretically predicted in 1960's [5]. To derive the mathematical expressions for parametric amplification in a aperiodic optical superlattice, the related formulas of optical parametric process in a homogeneous nonlinear medium should be briefly described here. Consider three optical plane waves with the frequencies ω_1, ω_2, and ω_3 ($\omega_3 = \omega_2 + \omega_1$), the equations governing the propagation of electromagnetic waves are written as

$$\begin{aligned}
\frac{dE_1}{dx} &= -\frac{\sigma_1}{2}\sqrt{\frac{\mu}{\epsilon_1}}E_1 - \frac{i\omega_1}{2}\sqrt{\frac{\mu}{\epsilon_1}}d_{33}E_3E_2^*e^{-i\Delta kx} \\
\frac{dE_2^*}{dx} &= -\frac{\sigma_2}{2}\sqrt{\frac{\mu}{\epsilon_2}}E_2^* + \frac{i\omega_2}{2}\sqrt{\frac{\mu}{\epsilon_2}}d_{33}E_1E_3^*e^{i\Delta kx} \\
\frac{dE_3}{dx} &= -\frac{\sigma_3}{2}\sqrt{\frac{\mu}{\epsilon_3}}E_3 - \frac{i\omega_3}{2}\sqrt{\frac{\mu}{\epsilon_3}}d_{33}E_1E_2e^{i\Delta kx},
\end{aligned} \tag{18}$$

where $\Delta k = k_3 - k_1 - k_2$, and σ_i (ϵ_i) is the loss coefficient (permittivity of crystal) for ω_i $(i = 1, 2, 3)$; μ is the magnetic permeability in vacuum. It is noted that these equations are coupled to each other via the nonlinear coefficient d_{33}.

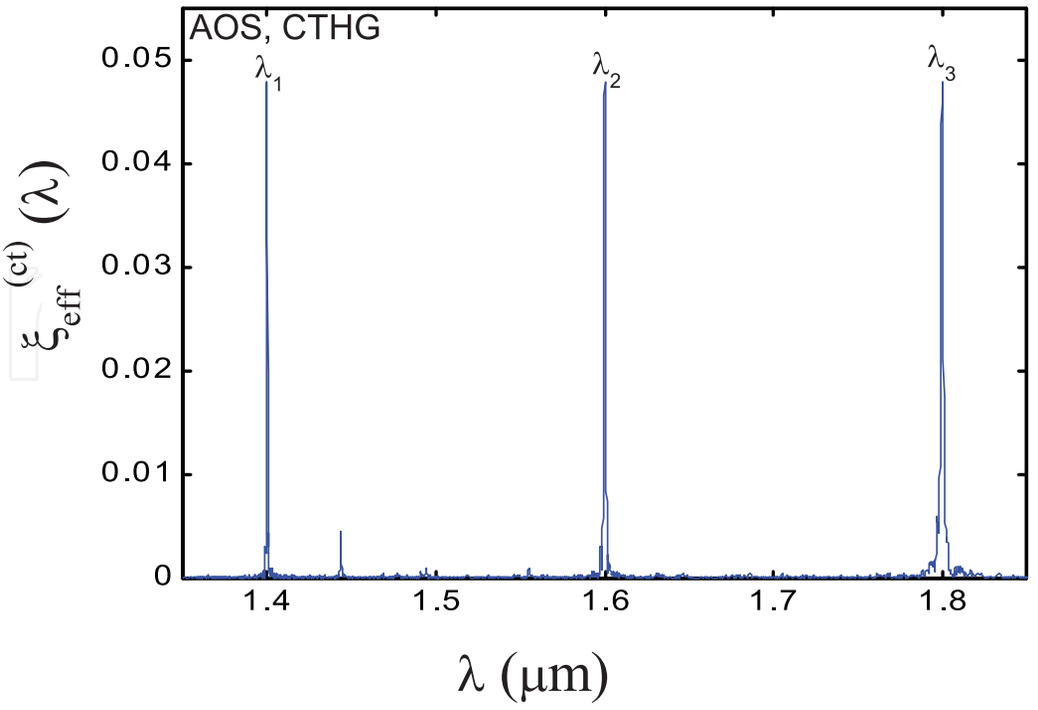

Figure 5. Calculated result for the constructed aperiodic optical superlattice that implements the coupled THG for three wavelength with an identical nonlinear coefficient.

Introducing a new field variable

$$A_i = \sqrt{\frac{n_i}{\omega_i}} E_i, \quad i = 1,2,3, \tag{19}$$

with n_i is the refraction index of crystal at $\omega_i (i = 1,2,3)$ and assuming the loss coefficients are negligible small, we can rewrite the first two equations in Equation 18 as

$$\begin{aligned} \frac{dA_1}{dx} &= -\frac{ig}{2} A_2^* e^{-i(\Delta k)x} \\ \frac{dA_2^*}{dx} &= +\frac{ig}{2} A_1 e^{i(\Delta k)x}, \end{aligned} \tag{20}$$

where

$$g = \sqrt{(\frac{\mu}{\epsilon_0})\frac{\omega_1 \omega_2}{n_1 n_2}} d_{33} E_3(0),$$

where ϵ_0 is permittivity of vacuum. In this derivation, we have used the approximation of small signal. In addition, we assume that $\omega_1 |A_1(x)|^2$ and $\omega_2 |A_2(x)|^2$ both remain small compared with $\omega_3 |A_3(0)|^2$ throughout the interaction region, thus $A_3(x)$ can be regarded as a constant. As the meaningful quantity is the relative phase between A_1 and A_3, therefore, we can set $A_3(0)$ to be real. Therefore, the relationship between the field variables $A_1(x)$, $A_2(x)$ and $A_1(x_0)$, $A_2(x_0)$ in homogeneous medium can be expressed as follows:

$$\begin{pmatrix} A_1(x) \\ A_2^*(x) \end{pmatrix} = \begin{pmatrix} M_{11} & M_{12} \\ M_{21} & M_{22} \end{pmatrix} \begin{pmatrix} A_1(x_0) \\ A_2^*(x_0) \end{pmatrix}, \tag{21}$$

where

$$M_{11} = e^{-i(\Delta k/2)(x-x_0)}\left[cosh(b(x-x_0)) + \frac{i(\Delta k)}{2b}sinh(b(x-x_0))\right],$$
$$M_{12} = e^{-i(\Delta k/2)(x-x_0)}e^{-i\Delta k x_0}\left[-i\frac{g}{2b}sinh(b(x-x_0))\right],$$
$$M_{21} = M_{12}^*,$$
$$M_{22} = M_{11}^*,$$

and

$$b = 0.5\sqrt{g^2 - (\Delta k)^2}. \tag{22}$$

Equations 21 and 22 tell that only when b is a real number, the signal and idler lights can be amplified. It requires that g must be greater than Δk. If the wavelengths of the pump and signal lights are selected as $1.064\mu m$ and $1.78\mu m$, respectively, Δk has the value of $0.20\mu m^{-1}$. Even considering the largest nonlinear coefficient $d_{33} = 21.6pm/V$ of $LiNbO_3$, it also requires the intensity of pump light being larger than $1.35 \times 10^{17} W/m^2$, which is impossible in practical applications.

For the aperiodic optical superlattice with block thickness of Δx, the coordinate of each blocks can be denoted by $x_q = q\Delta x$, for $q = 0, 1, 2, 3....N$, N is the total number of blocks in sample. Since d_{33} for each unit block remains constant, therefore, Equations 21 and 22 are still valid within each block. By using the transfer matrix method, the total transfer matrix can be established by cascading individual matrix associated with each block in sequence. For instance, the transfer matrix for the $(q+1)$th block from its left interface at x_q to its right interface at x_{q+1} can be expressed as

$$\begin{pmatrix} A_1(x_{q+1}) \\ A_2^*(x_{q+1}) \end{pmatrix} = \begin{pmatrix} M_{11} & M_{12} \\ M_{21} & M_{22} \end{pmatrix} \begin{pmatrix} A_1(x_q) \\ A_2^*(x_q) \end{pmatrix} = M(x_q \to x_{q+1}) \begin{pmatrix} A_1(x_q) \\ A_2^*(x_q) \end{pmatrix} \tag{23}$$

where

$$M_{11} = e^{-i(\Delta k/2)\Delta x_q}\left[cosh(b(x_q)\Delta x_q)) + \frac{i(\Delta k)}{2b(x_q)}sinh(b(x_q)\Delta x_q)\right],$$
$$M_{12} = e^{-i(\Delta k/2)\Delta x_q}e^{-i\Delta k x_q}\left[-i\frac{g(x_q)}{2b(x_q)}sinh(b(x_q)\Delta x_q)\right],$$
$$M_{21} = M_{12}^*,$$
$$M_{22} = M_{11}^*,$$

and

$$\Delta x_q = x_{q+1} - x_q. \tag{24}$$

Finally, the total transfer matrix reads

$$\begin{pmatrix} A_1(x_N) \\ A_2^*(x_N) \end{pmatrix} = \begin{pmatrix} M_{11}^{tot} & M_{12}^{tot} \\ M_{21}^{tot} & M_{22}^{tot} \end{pmatrix} \begin{pmatrix} A_1(x_0) \\ A_2^*(x_0) \end{pmatrix} = M^{tot}(x_0 \to x_N) \begin{pmatrix} A_1(x_0) \\ A_2^*(x_0) \end{pmatrix},$$

where

$$M^{tot}(x_0 \to x_N) = \Pi_{q=0}^{N-1} M(x_q \to x_{q+1}). \tag{25}$$

The initial conditions are known as $A_1(0)$ and $A_2^*(0)$ at $x_0 = 0$. In the general case, the initial idler wave $A_2(0)$ is considered as zero, so after signal wave passes through the aperiodic optical superlattice once, it is amplified by $G = M_{11}^{tot}$ times, therefore, G is the so–called amplification coefficient of the signal wave.

In the case of aperiodic optical superlattice, $\tilde{d}(x_q)$ varies with x_q, so g is a function of x_q as

$$g(x_q) = \sqrt{\left(\frac{\mu}{\epsilon_0}\right)\frac{\omega_1\omega_2}{n_1 n_2}}|d_{33}|\widetilde{d}(x_q)E_3(0). \tag{26}$$

Owing to $\tilde{d}^2(x_q) = 1$, the sign modulation of $\tilde{d}(x_q)$ does not bring any effect on b. However, $g(x_q)$ appearing in the transfer matrix is feeling to this sign modulation alone. Consequently, it is expected that the modulated structure may bring some benefits due to considerable effect of the sign modulation of $\tilde{d}(x_q)$ on parametric amplification process. In the case of multiple wavelengths parametric amplification, the situation becomes much more complicated, and it belongs to solving an inverse source problem.

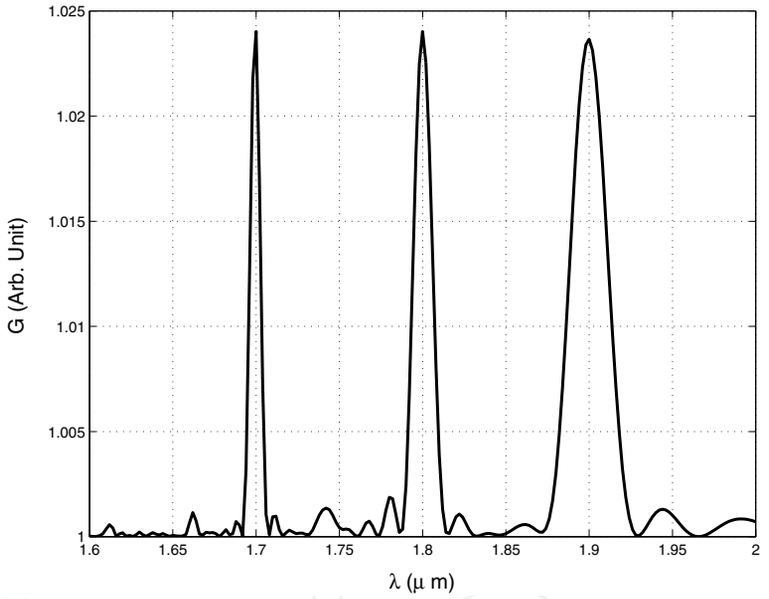

Figure 6. Calculated result for the constructed aperiodic optical superlattice that implements the parametric amplification for three wavelengths with an identical amplification coefficient.

The optimization design of aperiodic optical superlattice served as parametric amplifier for multiple wavelengths with identical amplification coefficient $G(\lambda_\alpha)$ is carried out. Three signal wavelengths λ_α are selected as $1.70\mu m$, $1.80\mu m$, and $1.90\mu m$. The pump intensity is $I_p = 10^{10} W/m^2$. Considering the practical technique for poling and dispersion of crystal, thickness of unit block $\Delta x = 8\mu m$ is selected in the simulation. The objective function for the SA algorithm is chosen as

$$E = \sum_{\alpha} |G_0 - G(\lambda_\alpha)| + \beta \left[max\{G(\lambda_\alpha)\} - min\{G(\lambda_\alpha)\} \right], \tag{27}$$

where β is a adjustable parameter taking a value of $0.3 \sim 3$. In multiple wavelengths parameter amplification, there is a trade-off between the amplification coefficients and uniformity, adjusting the value of β can balance them. Figure 6 exhibits the calculated

amplification coefficient as a function of wavelength for signal light. There exist three strong expected peaks and some small dense oscillation as background, satellite peaks are quite low. The amplifier coefficients are 1.0240, 1.0240, and 1.0237 for signal wavelengths $1.7\mu m$, $1.8\mu m$, and $1.9\mu m$, respectively. The average value $< G(\lambda_\alpha) >$ is 1.0239 and the maximal relative deviation is $\Delta G = [max\{G(\lambda_\alpha)\} - min\{G(\lambda_\alpha)\}]/ < G(\lambda_\alpha) >= 2.9 \times 10^{-4}$. These data show that the constructed aperiodic optical superlattice can meet the predefined requirement well.

3. Design of photonic crystal devices

Photonic crystals have attracted extensive attentions in the past decades. Two remarkable characters of the photonic crystals are photonic band gaps (PBGs) and defect states [6]. Based on these two characters, many devices can be designed.

3.1. Photonic crystal device for multiple wavelengths filtering

By inserting photonic quantum–wells (PQWs) into an ideal photonic crystal, a series of the discrete defect states may be created and they provide the function of multiple channeled filtering. Many researches have been reported on how to generate the defect states. However, the frequencies of the defect states cannot be changed with freedom. In practice, the favorable design of optical multiple channeled filters need to pass arbitrarily preassigned frequencies. In this section, the issue of designing the specific PQWs which have the preassigned filtering channels is discussed. The aperiodic PQWs (APQWs) are sandwiched by two finite-length ideal photonic crystals, which consist of two alternately stacked layers A and B with different dielectric constants of ε_A and ε_B, respectively. Their thicknesses are denoted by d_A and d_B, respectively, and $a = d_A + d_B$ is the lattice constant of the one-dimensional (1D) photonic crystal. The APQWs are composed of two different alternately stacked basic constituent layers with the dielectric constants of ε_C and ε_D. However, the thickness of each individual layer may not be equal and the individual layer thickness is determined by the merits of the desirable filters.

The transmission spectrum of designed APQW structures is calculated by using the transfer-matrix method. The transfer-matrix in each individual layer can be obtained by solving the Maxwell equations with a combination of boundary conditions. For a normally incident EM plane wave with the TE polarization, the transfer-matrix for the j-th layer is given by

$$\widehat{M}_j = \widehat{G}_{j+1}^{-1} \widehat{G}_j \widehat{P}_j, \tag{28}$$

where $j \in \{1, 2, ..., N\}$ for N number of layers. $\widehat{G}_j$ is the transfer matrix. The propagating matrix $\widehat{P}_j$ reads

$$\widehat{P}_1 = \begin{pmatrix} 1 & 0 \\ 0 & 1 \end{pmatrix}, \quad j = 1 \tag{29}$$

for air at the most left-hand side of the sample and

$$\widehat{P}_j = \begin{pmatrix} \exp(ik_j d_j) & 0 \\ 0 & \exp(-ik_j d_j) \end{pmatrix}, \quad j = 2, 3, 4... \tag{30}$$

for the jth layer in sample. $\widehat{G}_j$ reads

$$\widehat{G}_j = \begin{pmatrix} 1 & 1 \\ \sqrt{\varepsilon_j} & -\sqrt{\varepsilon_j} \end{pmatrix}, \tag{31}$$

where d_j denotes the thickness of the j-th layer, $k_j = 2\pi\sqrt{\varepsilon_j}/\lambda$, ε_j is the dielectric constant of the j-th layer; λ the wavelength of the incident light wave in vacuum. Thus, the total transfer matrix can be obtained by multiplying all individual transfer matrixes in sequence. The transmission and reflection coefficients of EM waves of the sample can be calculated from

$$\begin{pmatrix} t_n \\ r_n \end{pmatrix} = \prod_j \widehat{M}_j \begin{pmatrix} t_1 \\ r_1 \end{pmatrix}, \tag{32}$$

for instance, the transmission probability is given by

$$T = \sqrt{\frac{\varepsilon_n}{\varepsilon_1}} \left| \frac{t_n}{t_1} \right|^2. \tag{33}$$

For the wave which is not normal incident or TM mode, the similar approach can be used to obtain the transmission probability.

To design the APQW for producing specified defect states located at the preset frequencies $\omega_\alpha^{(0)}$ within a given range of $[\omega_a \quad \omega_b]$, a perfect PC should be selected to serve as the prototype photonic crystal, into which the APQW is implanted. It is required that the chosen prototype PC should have an appropriate PBG located at this frequency range and with a certain width, not narrower than the range of $[\omega_a \quad \omega_b]$. After determining this prototype PC, the APQW structure is determined by using the SA algorithm. The objective function is defined as

$$O = \sum_\alpha \sum_s |\omega_\alpha^{(o)} - \omega_\alpha^{(s)}|, \quad \omega_\alpha^{(o)}, \omega_\alpha^{(s)} \in [\omega_{\alpha-1}, \quad \omega_\alpha], \quad \alpha = 1, 2, 3.... \tag{34}$$

with

$$\omega_0 (= \omega_a) < \omega_1^o < \omega_1 < .... < \omega_{\alpha-1} < \omega_\alpha^o < \omega_\alpha (= \omega_b), \tag{35}$$

where $\omega_\alpha^{(s)}$ denotes the frequencies of the defect states appearing in $[\omega_{\alpha-1}, \omega_\alpha]$, which are generated in every routed configuration of the APQW during the SA routine. ω_α denote a series of the frequencies to partition the whole region of $[\omega_a, \omega_b]$ into several subregions. In each subregion, only one of the preassigned confined states appears. For instance, $\omega_\alpha^{(o)}$ is located in the subregion of $[\omega_{\alpha-1}, \omega_\alpha]$. In the SA routine, more than one defect states may occur in one subregion, thus, s may be larger than 1, therefore, the sum over s should be take into account. The optimal design of the APQWs corresponds to a search for the minimum of O. The sandwiched part in the sample is divided into n unit blocks with the thickness δd; the dielectric constant of each individual block is chosen as one of the binary of ε_C and ε_D, decided by the SA algorithm.

An APQW is design for achieving two channeled filtering in a given range of $[0.352 \quad 0.506](2\pi c/a)$, c is the speed of light in the vacuum. The dielectric constants are selected as $\varepsilon_A = \varepsilon_C = 13.0$ and $\varepsilon_B = \varepsilon_D = 1.0$. The thicknesses of the constituent layers A and B in the prototype PC are set to be $d_A = d_B = 0.5a$, thus, the second PBG of the prototype PC just is located at $[0.352 \quad 0.506](2\pi c/a)$. In the following calculations, five AB layers, $(AB)_5$,

on either side of the APQWs are employed. The sandwiched part is divided into $n = 100$ blocks and the thickness of the basic block $\delta d = 0.02a$ is selected. Two filtering frequencies are preassigned as $\omega_1^{(o)} = 0.420(2\pi c/a)$ and $\omega_2^{(o)} = 0.480(2\pi c/a)$. The transmission spectrum of the designed sample is displayed in Fig. 7. The frequency increment in the scan is taken as $\delta\omega = 1.0 \times 10^{-5}(2\pi c/a)$ to ensure that any unwanted extra stray frequency peak does not occur. Two dashed vertical lines remark the positions of the second PBG of the prototype $(AB)_5$ photonic crystal. It is evident that there exist only two expected defect states in the desired frequency range. The frequencies of the defect states accord exactly with the preset values. Their transmittances are 0.90 and 0.86 for $\omega_1 = 0.420(2\pi c/a)$ and $\omega_2 = 0.480(2\pi c/a)$, respectively.

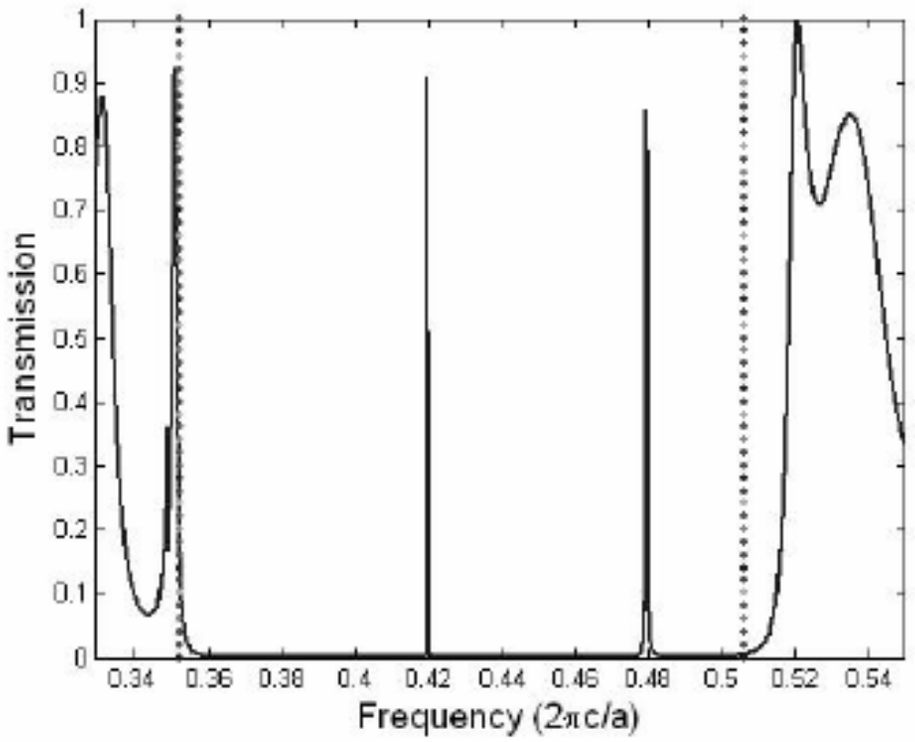

Figure 7. Transmission spectrum of the designed APQW sample for two channeled filtering at the preset frequencies of $\omega_1^{(o)} = 0.420$ and $\omega_2^{(o)} = 0.480(2\pi c/a)$.

3.2. Photonic crystal device for multiple wavelengths' second harmonic generation

When a defect is introduced into a perfect photonic crystal, the defect mode will appear in the band gap. Furthermore, the light with the frequency corresponding to the defect mode will be located around the defect layer; the intensity of the located wave has been improved 3-4 orders comparing with the intensity of the incident wave. Therefore, if a nonlinear material is used as the defect medium, the nonlinear effect can be greatly enhanced. It was found that when the frequency of the fundamental wave (FW) was tuned to the defect state, the SHG can be greatly enhanced. Due to the strong localization, low group velocity, and spatial phase locking in the PC, the giant enhancement of SHG for each FW has been achieved.

For simplicity, a one-dimensional layer structure is used as the sample. The incident wave is normally impinged upon the surface of the sample. For the $l-th$ layer, the electric field $E_l^{(1)}$ ($E_2^{(1)}$) of the FW (SHG), neglecting the pump power depletion, satisfies the following equations.

$$\left[\frac{d^2}{dz^2}+k_l^{(1)2}\right]E_l^{(1)}(z)=0, \tag{36}$$

$$\left[\frac{d^2}{dz^2}+k_l^{(2)2}\right]E_l^{(2)}(z)=-k_{20}^{(2)2}\chi^l(z)E_l^{(1)2}(z), \tag{37}$$

where $k_l^{(1)}=n_l^{(1)}k_{10}$, $k_l^{(2)}=n_l^{(2)}k_{20}$, $k_{10}=\omega/c$, $k_{20}=2\omega/c$, ω is the frequency of the FW, $n_l^{(1)}$ ($n_l^{(2)}$) is the refractive index of the $l-th$ layer for the wavelength of FW (SHG), c is the velocity of the light in vacuum and χ^l is the nonlinear optical coefficient of the $l-th$ layer. The solution of Equation 36 has the form

$$E_l^{(1)}(z)=A_l^{(1)}e^{ik_l^{(1)}(z-z_{l-1})}+B_l^{(1)}e^{-ik_l^{(1)}(z-z_{l-1})}, \tag{38}$$

where $A_l^{(1)}$ and $B_l^{(1)}$ represent the amplitudes of forward and backward FW at interface, respectively. Utilizing the continuous condition at each interface, the transfer matrix method, and the initial conditions ($A_l^{(1)}=1$ and $B_N^{(1)}=0$), the electric field of the FW in each layer can be obtained. N is the total number of layers in the sample.

Similarly, the SHG electric field in the $l-th$ layer of photonic crystal can be expressed as

$$\begin{aligned}E_l^{(2)}(z)=\ & A_l^{(2)}e^{ik_l^{(2)}(z-z_{l-1})}+B_l^{(1)}e^{-ik_l^{(1)}(z-z_{l-1})}+C_{21}e^{i2k_l^{(1)}(z-z_{l-1})}+C_{22}e^{-i2k_l^{(1)}(z-z_{l-1})}\\ & -\frac{2k_{20}^2\chi_l}{k_l^{(2)2}}A_l^{(1)}B_l^{(1)},\end{aligned} \tag{39}$$

$A_l^{(2)}$ and $B_l^{(2)}$ represent the amplitudes of the forward and backward SHGs at interface, respectively. C_{21} and C_{22} can be obtained as

$$\begin{aligned}C_{21}&=\frac{-k_{20}^2\chi_l A_l^{(1)2}}{k_l^{(2)2}-4k_l^{(1)2}},\\ C_{22}&=\frac{-k_{20}^2\chi_l B_l^{(1)2}}{k_l^{(2)2}-4k_l^{(1)2}}.\end{aligned} \tag{40}$$

Using the initial conditions $A_1^{(2)}=0$, $B_N^{(2)}=0$, the electric field of the SHG at each interface can be derived. The conversion efficiencies of the forward and backward SHG waves are defined respectively as follows

$$\eta_{forth}^{(2)}=\frac{n_N^{(2)}|A_N^{(2)}|^2}{n_1^{(1)}|A_1^{(1)}|^2},\eta_{back}^{(2)}=\frac{|B_1^{(2)}|^2}{|A_1^{(1)}|^2}. \tag{41}$$

As an example, the photonic crystal structure that can implement multiple wavelengths SHG is designed. The PQWs gives localized states at the frequencies of the FW and SHG,

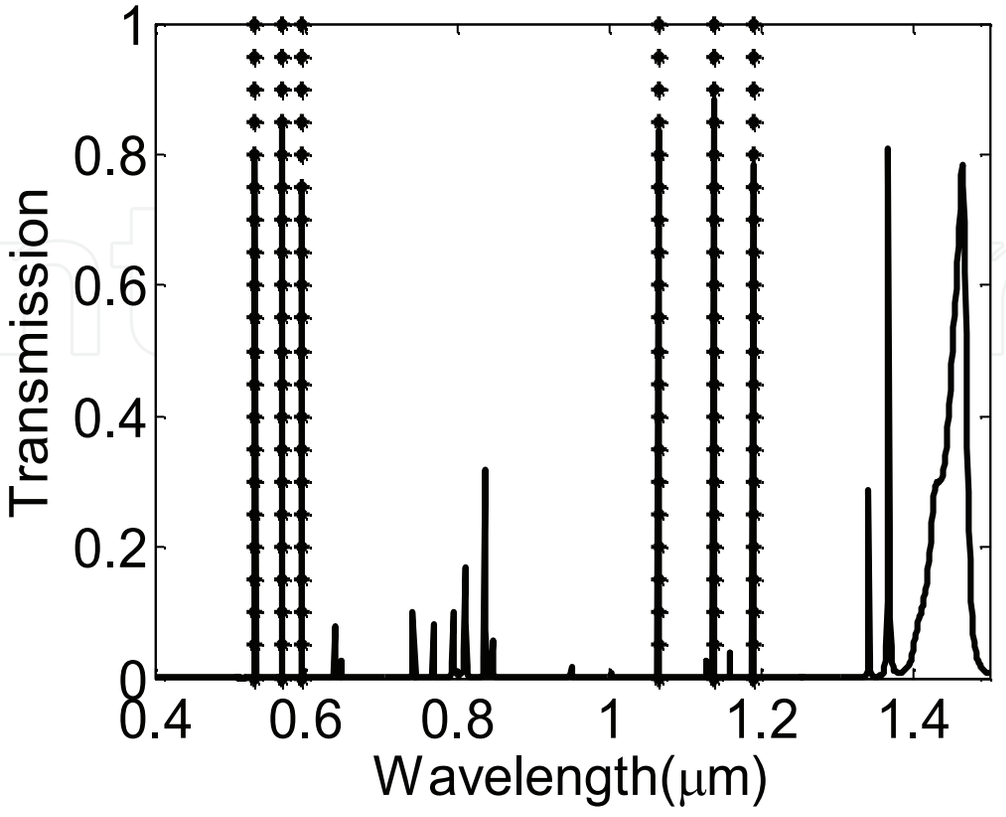

Figure 8. Transmission spectrum of the designed photonic quantum well structure. The dash lines indicate $\lambda_{1,1} = 1.064\mu m$, $\lambda_{1,2} = 1.136\mu m$, $\lambda_{1,3} = 1.188\mu m$, $\lambda_{2,1} = 0.532\mu m$, $\lambda_{2,2} = 0.568\mu m$, and $\lambda_{2,3} = 0.594\mu m$.

respectively. The preset wavelengths of FWs are $\lambda^o_{1,1} = 1.064\mu m$, $\lambda^o_{1,2} = 1.136\mu m$, and $\lambda^o_{1,3} = 1.188\mu m$, and the wavelengths of the corresponding second harmonics are $\lambda^o_{2,1} = 0.532\mu m$, $\lambda^o_{2,2} = 0.568\mu m$, and $\lambda^o_{2,3} = 0.594\mu m$, respectively. The conversion efficiencies for three FWs are required to be nearly equal. The periodic structure $(AB)_5$ is selected as the prototype photonic crystal. A and B are $LiNbO_3$ and air, respectively. The widths of the A and B layers are selected as $d_A = 0.1814\mu m$ and $d_B = 0.1330\mu m$, respectively. This prototype photonic crystal has two band gaps $[0.916\mu m \quad 1.314\mu m]$ and $[0.482\mu m \quad 0.612\mu m]$. The FWs and SHGs are located in the two band gaps, respectively. Then a aperiodic structure is designed and insert into the prototype photonic crystals. The thickness of C and D unit cell is $d_C = d_D = 0.04\mu m$, the number of unit cells is 300. However, each cell is selected from C or D which is determined by the SA algorithm with an objective function as

$$O = \sum_{\alpha}\sum_{s}\sum_{k}\left[|\lambda^o_{\alpha,s} - \lambda^k_{\alpha,s}| + \beta_1|\eta^0 - \eta^{(k)}_{1,s}|\right] + \beta_2|max(\{\eta^{(k)}_{1,s}\}) - min(\{\eta^{(k)}_{1,s}\})| \qquad (42)$$

where

$$\begin{array}{c} \lambda^o_{1,s}, \lambda^{(k)}_{1,s} \in [\lambda_{1,s-1}, \lambda_{1,s}] \in [\lambda_a, \lambda_b], \\ \lambda^o_{2,s}, \lambda^{(k)}_{2,s} \in [\lambda_{2,s-1}, \lambda_{2,s}] \in [\lambda_c, \lambda_d], \\ \alpha = 1,2 \qquad\qquad s = 1,2,3,...., \end{array}$$

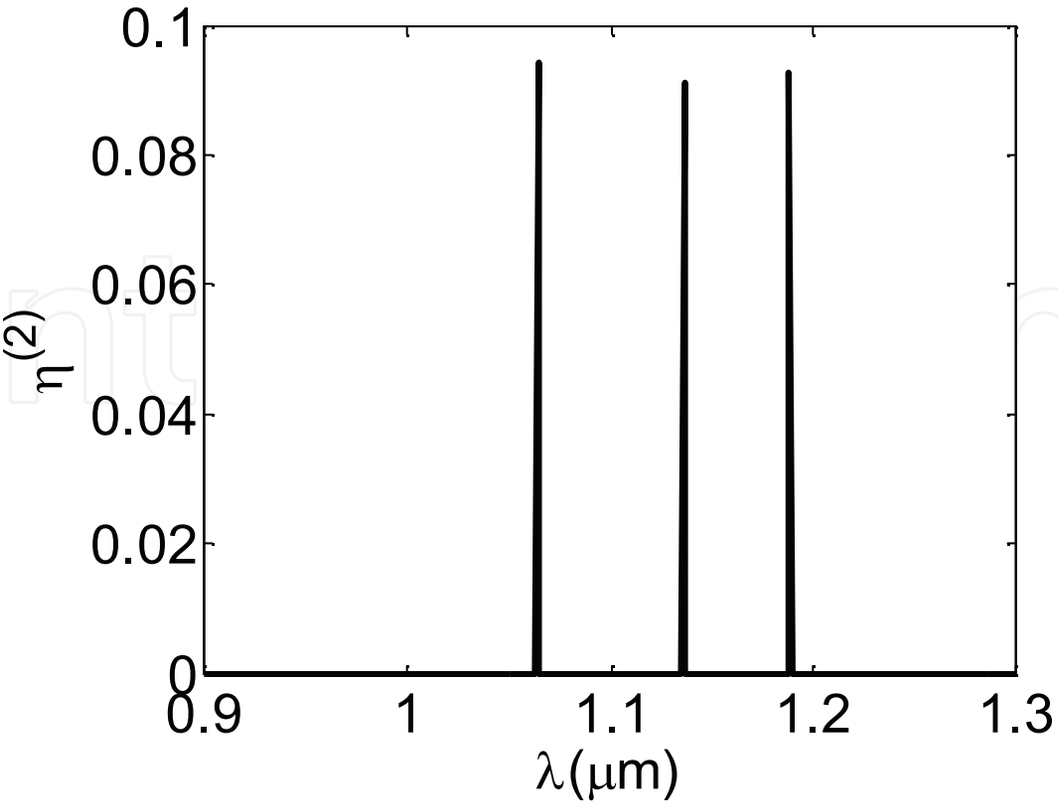

Figure 9. Wavelength dependence of the conversion efficiency of the photonic quantum well structure for the forward SHG.

with

$$\lambda_{1,0}(=\lambda_a) < \lambda^o_{1,1} < \lambda_{1,1} < \lambda^o_{1,2} < \lambda_{1,2} < ... < \lambda^o_{1,s} < \lambda_{1,s}(=\lambda_b);$$
$$\lambda_{2,0}(=\lambda_c) < \lambda^o_{2,1} < \lambda_{2,1} < \lambda^o_{2,2} < \lambda_{2,2} < ... < \lambda^o_{2,s} < \lambda_{2,s}(=\lambda_d).$$

β_1 and β_2 are two adjustable constants. $\lambda^{(k)}_{\alpha,s}$ and $\eta^k_{1,s}$ denote the wavelengths of the defected states and corresponding conversion efficiencies generated from every transit structure during the SA process. s is the number of the FW to be designed and it was selected as $s = 3$ in this work. The PQW structure is designed by the SA.

Figure 8 presents the transmission spectrum of the designed photonic quantum well structure. The band structure of the PC $(AB)_{10}$ is almost unchanged. The wavelengths designed appear at $\lambda_{1,1} = 1.064\mu m$, $\lambda_{1,2} = 1.136\mu m$, $\lambda_{1,3} = 1.188\mu m$, $\lambda_{2,1} = 0.532\mu m$, $\lambda_{2,2} = 0.568\mu m$, and $\lambda_{2,3} = 0.594\mu m$ respectively. They agree with the required wavelengths quite well.

The properties of the SHG for this structure is also investigated. The largest nonlinear coefficient d_{33} of $LiNbO_3$ is used for achieving high conversion efficiency. The intensity of the incident FW is selected as $0.021GW/m^2$ for each wavelength. The wavelength dependence of the SHG is shown in Fig. 9. Only three expected wavelengths appear. The conversion efficiencies of the forward SHGs are $\eta_1 = 0.0943$, $\eta_2 = 0.0912$, and $\eta_3 = 0.0926$, respectively. The conversion efficiencies have been enhanced nearly 10^3 time comparing with the periodically poled lithium niobate structure with identical length. The conversion efficiencies of the forward SHGs are nearly identical, which correspond to the designed aim well. Comparing with the structure with only the FW located at the defect state, the conversion efficiencies have also been mightily enhanced.

3.3. Photonic crystal device for multiple wavelengths' coupled third harmonic generation

For the coupled third harmonic generation, the electric field $E_l^{(1)}$ ($E_l^{(2)}$, $E_l^{(3)}$) of the FW (SHG, CTHG) for the $l-th$ layer must satisfy the following equations:

$$\left[\frac{d^2}{dz^2}+k_l^{(1)2}\right]E_l^{(1)}(z)=0, \tag{43}$$

$$\left[\frac{d^2}{dz^2}+k_l^{(2)2}\right]E_l^{(2)}(z)=-k_{20}^{(2)2}\chi_l(z)E_l^{(1)2}(z), \tag{44}$$

$$\left[\frac{d^2}{dz^2}+k_l^{(3)2}\right]E_l^{(3)}(z)=-2k_{30}^{(2)2}\chi_l(z)E_l^{(1)}(z)E_l^{(2)}(z), \tag{45}$$

where $k_l^{(1)}=n_L^{(1)}k_{10}$, $k_l^{(2)}=n_L^{(2)}k_{20}$, $k_l^{(3)}=n_L^{(3)}k_{30}$, $k_{10}=\omega/c$, $k_{20}=2\omega/c$, and $k_{30}=3\omega/c$ are wave vectors of the FW, SHG, and CTHG, respectively. ω is the frequency of the FW, $n_l^{(1)}$ ($n_l^{(2)}$, $n_l^{(3)}$) is the refractive index of the $l-th$ layer for the wavelength of FW (SHG, CTHG), c is the velocity of the light in vacuum and χ^l is the nonlinear optical coefficient of the $l-th$ layer. Similarly, the expression of CTHG electric field in the $l-th$ layer is

$$\begin{aligned}E_l^{(3)}(z)=&A_l^{(3)}e^{ik_l^{(3)}(z-z_{l-1})}+B_l^{(3)}e^{-ik_l^{(3)}(z-z_{l-1})}+C_{31}e^{i[k_l^{(1)}+k_l^{(2)}](z-z_{l-1})}+C_{32}e^{-i[k_l^{(1)}+k_l^{(2)}](z-z_{l-1})}\\&+D_{31}e^{i[k_l^{(1)}-k_l^{(2)}](z-z_{l-1})}+D_{32}e^{-i[k_l^{(1)}-k_l^{(2)}](z-z_{l-1})}+E_{31}e^{i3k_l^{(1)}(z-z_{l-1})}\\&+E_{32}e^{-i3k_l^{(1)}(z-z_{l-1})}+F_{31}e^{ik_l^{(1)}(z-z_{l-1})}+F_{32}e^{-ik_l^{(1)}(z-z_{l-1})},\end{aligned} \tag{46}$$

and all parameters in this equation can be expressed as

$$\begin{aligned}C_{31}&=\frac{-k_{30}^2\chi_l A_l^{(1)}A_l^{(2)}}{k_l^{(3)2}-(k_l^{(1)}+k_l^{(2)})^2}, & C_{32}&=\frac{-k_{30}^2\chi_l B_l^{(1)}B_l^{(2)}}{k_l^{(3)2}-(k_l^{(1)}+k_l^{(2)})^2},\\ D_{31}&=\frac{-k_{30}^2\chi_l A_l^{(1)}B_l^{(2)}}{k_l^{(3)2}-(k_l^{(1)}-k_l^{(2)})^2}, & D_{32}&=\frac{-k_{30}^2\chi_l A_l^{(2)}B_l^{(1)}}{k_l^{(3)2}-(k_l^{(1)}-k_l^{(2)})^2},\\ E_{31}&=\frac{-k_{30}^2\chi_l A_l^{(1)}C_{2l}}{k_l^{(3)2}-9k_l^{(1)2}}, & E_{32}&=\frac{-k_{30}^2\chi_l B_l^{(1)}C_{22}}{k_l^{(3)2}-9k_l^{(1)2}},\\ F_{31}&=\frac{-k_{30}^2\chi_l B_l^{(1)}C_{2l}}{k_l^{(3)2}-k_l^{(1)2}}+\frac{2k_{30}^2k_{20}^2\chi_l^{(2)}\chi_l A_l^{(1)2}B_l^{(1)}}{k_l^{(2)2}(k_l^{(3)2}-k_l^{(1)2})},\\ F_{32}&=\frac{-k_{30}^2\chi_l A_l^{(1)}C_{22}}{k_l^{(3)2}-k_l^{(1)2}}+\frac{2k_{30}^2k_{20}^2\chi_l^{(2)}\chi_l B_l^{(1)2}A_l^{(1)}}{k_l^{(2)2}(k_l^{(3)2}-k_l^{(1)2})}.\end{aligned} \tag{47}$$

By using the initial conditions $A_1^{(2)}=0$, $B_N^{(2)}=0$, $A_1^{(3)}=0$, and $B_N^{(3)}=0$, the electric fields of CTHG at each interface can be obtained. Therefore, the conversion efficiencies of the forward and backward waves are defined respectively as

$$\eta_{forth}^{(3)}=\frac{n_N^{(3)}|A_N^{(3)}|^2}{n_1^{(3)}|A_1^{(1)|^2}},\quad \eta_{back}^{(3)}=\frac{|B_1^{(3)}|^2}{|A_1^{(1)}|^2}. \tag{48}$$

Similarly, a prototype photonic crystal $(AB)_{10}$ is designed. The thicknesses of A and B layers are $d_A=0.2557\mu m$ and $d_B=0.1875\mu m$, respectively. Thus this photonic crystal has

three band gaps as $[\lambda_a = 1.283\mu m, \lambda_b = 1.835\mu m]$, $[\lambda_c = 0.667\mu m, \lambda_d = 0.848\mu m]$, and $[\lambda_e = 0.477\mu m, \lambda_f = 0.533\mu m]$. The double wavelengths CTHG is considered here, the preset wavelengths are $\lambda^O_{1,1} = 1.458\mu m$, $\lambda^O_{1,2} = 1.578\mu m$, $\lambda^O_{2,1} = 0.729\mu m$, $\lambda^O_{2,2} = 0.789\mu m$, $\lambda^O_{3,1} = 0.486\mu m$, and $\lambda^O_{3.2} = 0.526\mu m$, respectively. The object function in this case is similar with that for multiple wavelengths SHG. The transmission spectrum of the designed structure is shown in Fig. 10. The peak wavelengths appear at $\lambda_{1,1} = 1.458\mu m$, $\lambda_{1,2} = 1.578\mu m$, $\lambda_{2,1} = 0.729\mu m$, $\lambda_{2,2} = 0.789\mu m$, $\lambda_{3,1} = 0.486\mu m$, and $\lambda_{3,2} = 0.526\mu m$, respectively. They agree well with the required wavelengths. Figure 11 presents the dependence of conversion

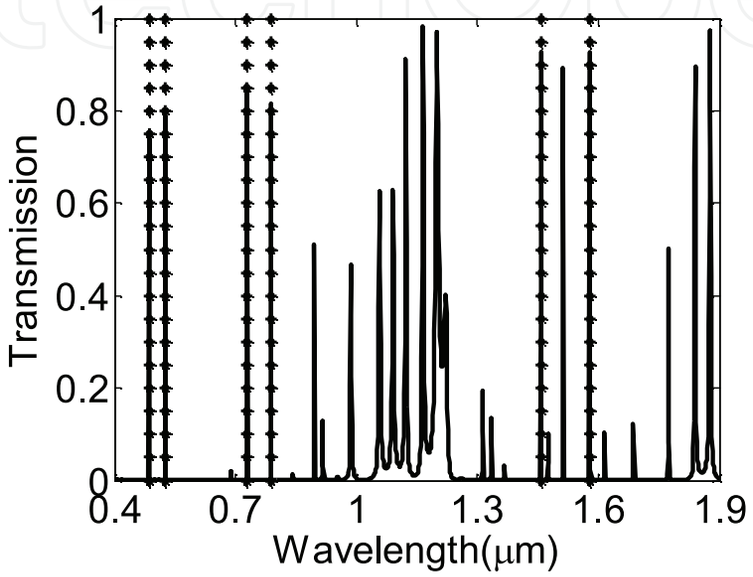

Figure 10. Transmission spectrum of the designed photonic quantum well structure for double wavelengths CTHG. The dashed lines represent $\lambda_{1,1} = 1.458\mu m$, $\lambda_{1,2} = 1.578\mu m$, $\lambda_{2,1} = 0.729\mu m$, $\lambda_{2,2} = 0.789\mu m$, $\lambda_{3,1} = 0.486\mu m$, and $\lambda_{3,2} = 0.526\mu m$, respectively.

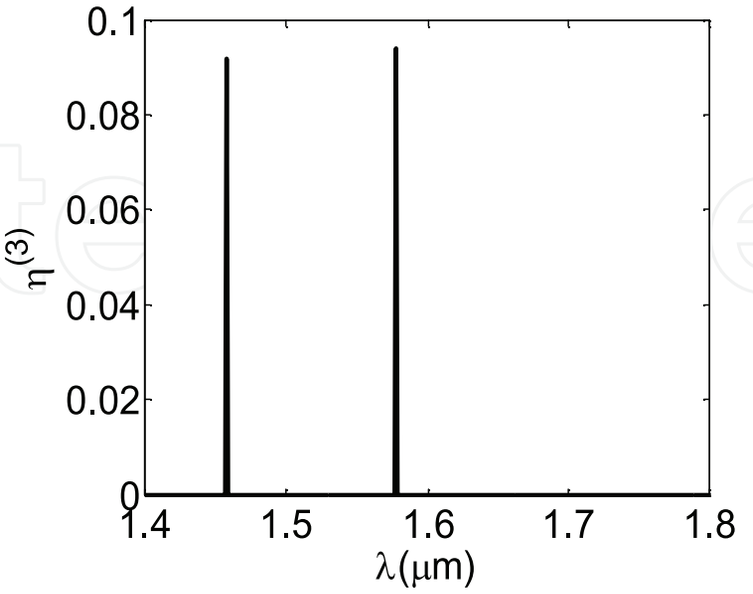

Figure 11. Conversion efficiency of the forward CTHG.

efficiency of the CTHG on the wavelength of FW of the designed structure. Only for the two preset wavelengths, the conversion efficiency is quite high. The conversion efficiencies are $\eta_{1,1} = 0.0917$ for $\lambda_{1,1} = 1.458\mu m$ and $\eta_{1,2} = 0.0938$ for $\lambda_{1,2} = 1.578\mu m$, the conversion efficiencies are nearly identical which corresponds to the required aim well.

4. Conclusion

In a conclusion, the SA algorithm is employed to design nonlinear frequency conversion devices. The basic design method is explained in detail. Some devices include multiple second harmonics generation devices, multiple coupled third harmonics generation devices, multiple channeled photonic crystal filters, multiple second harmonics photonic crystal devices, and multiple coupled third harmonics photonic crystal devices are designed using the proposed method. The designed devices can achieved preset goals well. It is expected that this new proposed method can provide a novel approach for nonlinear conversion devices design.

Author details

Yan Zhang
Beijing Key Lab for Terahertz Spectroscopy and Imaging
Key Laboratory of Terahertz Optoelectronics, Ministry of Education
Department of Physics, Capital Normal University, Beijing, 100048 China

5. References

[1] Yariv, A. & Yeh, A. (1984). *Optical Wave in Crystal*, Wiley, New York.
[2] Shen, Y. R. (1984). *The Principles of Nonlinear Optics*, Wiley, New York.
[3] Bloembergen, N. & Sievers, A. J. Nonlinear optical properties of periodic laminar structures, *Appl. Phys. Lett.*, Vol. 17 (No. 11) 483-485.
[4] Meyn, J. P. & Fejer, M. M. (1997). Tunable ultraviolet radiation by second-harmonic generation in periodically poled lithium tantalate, *Opt. Lett.*, Vol. 22 (No. 16) 1214-1216.
[5] Giordmaine, J. A. & Miller R. C. Tunable coherent parametric oscillation in $LiNbO_3$ at optical frequencies, *Phys. Rev. Lett.* Vol. 14 (No. 24) 973-976.
[6] Yablonobitch E. (1987). Inhibited spontaneous emission in solid-state physics and electronics, *Phys. Rev. Lett.* Vol. 58 (No. 20) 2059-2062.